# Highly stable gold nanolayer membrane for efficient solar water evaporation under a harsh environment

Idris Ibrahim[a], Dong Han Seo[a,b*], Myoung Jun Park[a], Alexander Angeloski[c], Andrew McDonagh[c], Avi Bendavid[d,e], Ho Kyong Shon[a,f], Leonard Tijing[a,f,*]

[a]Centre for Technology in Water and Wastewater, School of Civil and Environmental Engineering, University of Technology Sydney, PO Box 123, 15 Broadway, Sydney, NSW, 2007, Australia

[b]Energy Materials & Devices, Korea Institute of Energy Technology (KENTECH), Naju, Republic of Korea.

[c]School of Mathematical and Physical Sciences, University of Technology Sydney, Ultimo 2007, Australia

[d]CSIRO Manufacturing, 36 Bradfield Road, Lindfield, NSW, 2070, Australia.

[e]School of Materials Science and Engineering, University of New South Wales, Kensington, NSW, 2052, Australia

[f]ARC Research Hub for Nutrients in a Circular Economy, University of Technology Sydney, PO Box 123, 15 Broadway, Sydney, NSW, 2007, Australia

[*]Corresponding authors: D.H. Seo, dhseo@kentech.ac.kr; L. Tijing, leonard.tijing@uts.edu.au

## Highlights

- A novel strategy to fabricate a scalable gold nanolayer membrane is reported.
- The modified membrane demonstrates robust chemical and mechanical stability.
- High salt ion rejection of seawater was demonstrated.
- The gold nanolayer membrane showed high reusability and stability under wide pH ranges.

## Graphical abstract

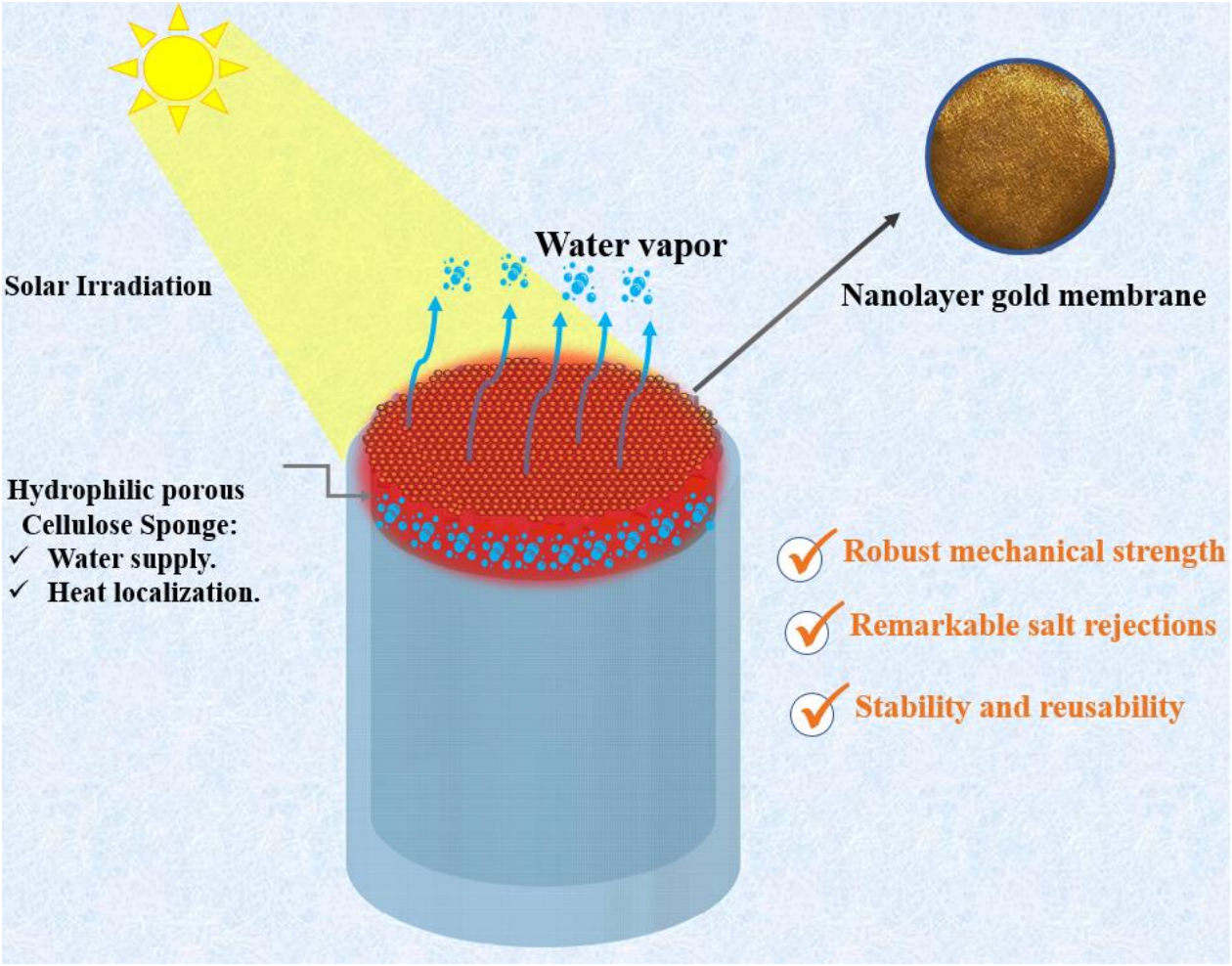

**Abstract**

Interfacial solar water evaporation has attracted tremendous attention for sunlight harvesting for water purification. However, salt formation and stability of the photothermal materials (PTMs) remain a challenge that need addressing before bringing this technology to real-world applications. In this work, a nanoscale thin film of gold (Au) on a polytetrafluoroethylene (PTFE) membrane has been prepared using a magnetic sputtering technique. The fabricated membrane displays a robust mechanical strength and chemical stability arising from the adhesiveness of the thin film Au nanolayer on the PTFE membrane as well as the chemical inertness of the noble metal PTM. The Au nanolayer/PTFE membrane with cellulose sponge substrate resulted in an evaporation rate of 0.88 kg $m^{-2}$ $h^{-1}$ under 1 sun intensity. Remarkable salt ion rejection of 99.9% has been obtained, meeting the required standard for drinking water. Moreover, the membrane exhibited excellent stability and reusability in natural seawater and high salinity brine (150 g/L) and even in severe conditions (acidic, basic, and oxidized). No noticeable salt formation was observed on the evaporator surface after the tests. These findings reveal promising prospects for using a magnetron sputtering technique to fabricate a stable photothermal membrane for seawater and high salinity brine desalination.

**Keywords:** Gold nanolayer membrane; photothermal conversion; solar water evaporation, desalination; reusability; harsh environment.

## 1. INTRODUCTION

In recent years, solar water evaporation (SWE) (also called solar steam generation) has attracted increased interest as a passive, decentralized, and sustainable desalination technology for use in inland and off-grid areas where freshwater is scarce and sunlight is abundant (Li et al., 2018a; Li et al., 2018b; Chen et al., 2021a). This is in contrast with the mainstream centralized desalination technologies like reverse osmosis that require big infrastructures and a high amount of fossil fuel-based energy sources (Ghafurian et al., 2020b; Li et al., 2021). Small-scale SWE system can generate over 10 kg $m^{-2}$ $day^{-1}$ of clean water and can be scaled up due to simplicity in setup and design (Li et al., 2020). In this study, we refer to SWE in the context of interfacial solar water evaporation. The technology is based on photothermal materials (PTMs) that absorb sunlight and convert it into heat at the air/water interface, which effectively vaporizes water at the solar absorber surface, then condenses it to generate clean water (Tao et al., 2018; Wu et al., 2019b; Ibrahim et al., 2020; Shi et al., 2020; Zhao et al., 2020c; Liu et al., 2021; Wang et al., 2021). However, salt crystallization on the evaporation area is the main issue that needs to be addressed to implement this technology for practical applications. This results in poor light absorption, which reduces the overall evaporation surface by blocking the water vapor channel, hence decreasing the water evaporation rate (Chen et al., 2021b; Ibrahim et al., 2021b; Peng et al., 2021). To date, various strategies have been proposed to overcome this issue by designing various PTMs including porous polymer materials (He et al., 2020; Wang et al., 2020), bioinspired microstructure materials (Huang et al., 2020a), Janus materials (Xu et al., 2018; Chen et al., 2020; Peng et al., 2021), and hydrophobic materials (Wei et al., 2021). However, the chemical stability and resistivity to harsh chemical conditions remains a question that must be addressed to ensure long-term stability.

Among the reported PTMs for SWE, noble metals such as gold nanoparticles have been used as firstly reported by Halas et al. in 2013 (Neumann et al., 2013), and have since attracted broad interest, which led to an increase in research activities related to SWE. Noble metals are known to exhibit excellent chemical stabilities under harsh environments such as for evaporation of source water with highly acidic and basic conditions (Hammer and Norskov, 1995; Badawy et al., 2010; Kiriarachchi et al., 2018). Previous studies on noble metal-based PTMs utilized either complicated or small-scale synthesis strategies (Zhang et al., 2019). Furthermore, the mechanical strength of their fabricated PTMs remains a challenge, hence hindering their practical implementation. Thus, a scalable strategy to allow the fabrication of nanoscale noble metal-based PTMs with excellent mechanical stability is essential for practical application of SWE.

Magnetron sputtering (MS) is a promising technique that enables the deposition of nanoscale thin film on various substrates (Grammatikopoulos et al., 2013). The method provides a cost-effective thin film coating at relatively low temperatures and can produce uniform thin film layers on large substrate areas with excellent adhesion (Greene, 2017; Barbosa et al., 2019). In the present study, a well-designed Au nanolayer on PTFE membrane surface fabricated by an MS technique for SWE application is demonstrated. Benefitting from the strong adhesion of the Au nanolayer on the PTFE membrane surface, the current approach results in a membrane with robust mechanical strength and excellent chemical stability even under harsh environments. The light absorption capability of our fabricated membrane covers the whole solar spectrum region. The designed solar evaporator of Au nanolayer-PTFE on cellulose sponge resulted in excellent salt ion rejection, meeting the required standard for drinking water. Furthermore, exceptional reusability and stability are demonstrated in natural seawater and harsh chemical conditions. Our findings reveal the novelty of magnetic sputtering methods for

scaling up highly stable PTMs with excellent salt resistance for long-term durability solar evaporators.

## 2. Materials and methods

### 2.1 Materials

Gold targets (Au >99.9% purity) were purchased from Kurt J. Lesker company. A commercial polytetrafluoroethylene (PTFE, 0.45 μm pore size) membrane was obtained from Ningbo and was used as a substrate for the formation of nanoscale thin film Au layer. A commercial cellulose sponge was purchased from a local supermarket, and was utilized as the insulator and floating support for the Au nanolayer membrane. Potassium hydroxide (KOH) was purchased from Merck; hydrochloric acid was bought from Chem-Supply, and sulfuric acid and nitric acid were received from Sigma Aldrich**.**

### 2.2. Fabrication of Au nanolayer membrane

Nanoscale Au thin films on PTFE membranes were formed using a magnetron sputtering system equipped with a 75 mm Au diameter target and power supply (AJA DCXS-750, Scituate, MA, USA). The high target purity was 99.99%. The distance between the target and the substrate (PTFE membrane) was set at 70 mm. The deposition system was equipped with rotary and cryogenic pumps and a controlled gas introduction system. A base pressure of $1x10^{-4}$ Pa was attained in the chamber before the deposition. Argon gas was introduced into the chamber prior to the deposition process. The deposition pressure (1.0 Pa) was set independently of the gas flow by adjusting a throttle valve. DC power was set at 100 W. The deposition time was 4 min, and the thickness of deposition nanolayer thin film was 50 nm (Ghafurian et al., 2020a) and the change in the mass loading of the PTFE membrane after the gold nanolayer deposition was 45 $\mu g/cm^2$.

### 2.3 Characterization

The structure and the morphology of pristine PTFE and Au nanolayer membrane was investigated using field emission scanning electron microscopy (FE-SEM, Zeiss Supra 55VP) at an accelerated voltage of 10 kV. The surface wetting ability of the samples was investigated by Theta Lite 100 (Attension) using a sessile drop method. A volume of 10 µL water droplet was vertically dropped on the substrate surface. The light absorption characteristics of the pristine PTFE and Au nanolayer membranes were measured at a wavelength range of 300-2500 nm (i.e., ultraviolet-visible-near-infrared regions) using a spectrophotometer equipped with an integrating sphere (950 PerkinElmer Lambda). Infrared (IR) images and surface temperatures were recorded using an infrared camera (FLIR, E6). The concentrations of the positively charged ions ($K^+$, $Na^+$, $Mg^{2+,}$ and $Ca^{2+}$) in seawater before and after purification were measured using an inductively coupled plasma mass spectrometer (ICP-MS, Agilent 7900), while the negatively charged ions ($NO_3^-$, $Cl^{-,}$ and $SO_4^{-2}$) were measured using ion chromatography (IC) (Thermo Fisher, Australia).

### 2.4 Solar water evaporation test

The SWE set-up consisted of a solar simulator (PLS-SXE300) with a standard AM 1.5G filter, a precision analytical weighing balance (IC-PX84/E, Ohaus, 0.1 mg accuracy) connected to a computer, an infrared camera (FLIR E6), and Type-K thermocouples (RS PRO: RS172TK) (**Fig. S1**). The Au/PTFE membrane solar evaporator (diameter = 4.5 cm) placed on top of a cellulose sponge with a thickness of 1.2 cm (wet) (**Fig. S2**), was floated on a 100 ml beaker filled with 80 mL deionized water (DIW). The effect of the cellulose sponge was investigated at different thicknesses (0.6, 1.2 cm and 1.6 cm). During the experiment, simulated sunlight at an intensity of 1 sun (1 kW $m^{-2}$) was illuminated on the solar evaporator which was placed on an electronic balance. The change in weight with respect to time was continuously recorded at 4 min interval, with each evaporation experiment lasting for 1 h. Changes in membrane surface

temperature were measured by an IR camera at various intervals, and a thermocouple was used to measure the bulk water temperature changes. SWE experiments at dark condition (without simulated light) were also carried out. Pristine PTFE membrane without gold thin film coating was also checked for its SWE performance, which served as the control for comparison. All experiments were carried out at room temperature of 22 ± 2 $^{o}$C and humidity of ~52.5%.

### 2.5 Solar water desalination and stability test under harsh environment

The potential of our Au nanolayer membrane for water desalination was evaluated by treating a real seawater collected from Cronulla Beach, Sydney, Australia and similar protocols for SWE tests were followed. In addition, a high salinity NaCl brine solution (at 150 g/L) was also prepared. The stability of the gold PTMs was evaluated under a harsh environment utilizing acidic (0.1 M $H_2SO_4$), basic (0.1 M KOH), and oxidizing conditions (0.1 M $HNO_3$), with respective ionic strengths (*I*) of 0.3 M, 0.1 M, and 0.1 M (Zhao et al., 2020b). During the water purification tests, the evaporated water was collected and analyzed using ICP and IC techniques to measure the ions of the feedwater and the collected water. In addition, cycling stability tests (10 cycles) were demonstrated.

## 3. Results and discussion

### 3.1 Characterization of Au nanolayer-PTFE membrane

**Fig 1.** shows the pristine PTFE membrane and the fabricated Au nanolayer films coated PTFE membranes. A magnetron sputtering process was used to uniformly coat thin films of gold onto PTFE membranes. The duration of the coating process was 4 min with film thickness of 50 nm. This type of coating process ensures quick, highly scalable, and uniform deposition of materials in a single step without the use of chemicals making it a practical fabrication approach. This technology enables the fabrication of Au nanolayer membranes in large areas, which is vital

for practical applications (**Fig. S3**). A PTFE membrane was chosen as the substrate due to its good mechanical strength, flexibility, chemical stability and high-temperature resistance (Chang et al., 2018). During the magnetron sputtering process, strong physisorption was expected between the partially ionized Au particles and the modified PTFE membrane surface which led to their good adhesion with each other (Pinho and Piedade, 2013). As illustrated in **Fig. 1a-c,** after deposition of the Au nanolayer, the circular white membrane top surface (inset of Fig 1a) acquired a gold color, signifying the successful coating of the Au nanolayer. The coated membranes displayed strong adherence of the thin-layer Au to the PTFE membrane. The modified membranes can easily be folded and returned to their original state without detachment of the coating or membrane damage (**Fig. 1d**). These features are beneficial for the development of scalable and effective PTM for solar water evaporators.

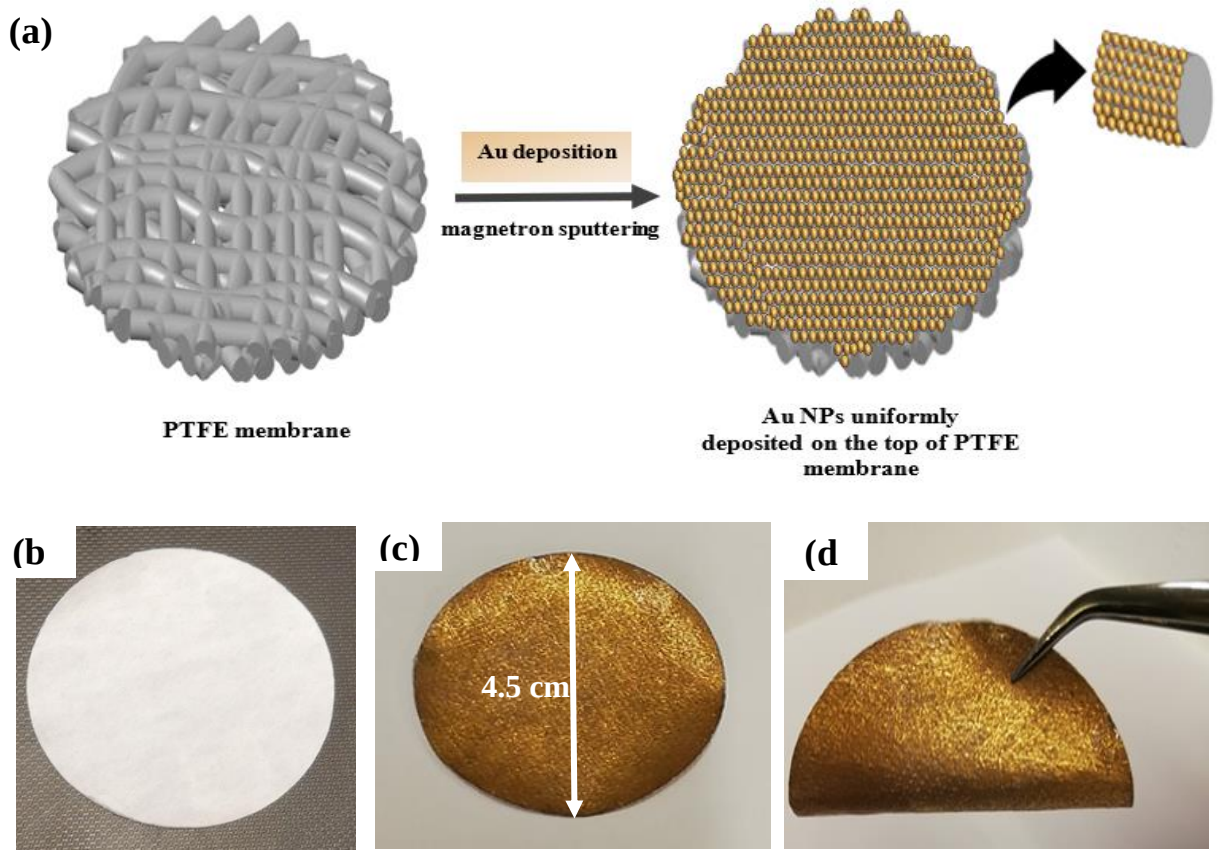

**Fig. 1** (a) Schematic illustration of gold deposition on a pristine PTFE membrane substrate. Images showing the (b) pristine PTFE membrane, (c) gold-coated PTFE membrane, and (d) the flexibility of the Au-PTFE membrane.

The structural morphology, elemental compositions, surface analysis and wettability of the fabricated Au nanolayer were examined. SEM images reveal that the surface morphology of the pristine PTFE membrane contains unequal-length extended holes with open and distributed channels (**Fig. S4**). After gold deposition, a homogeneously distributed gold layer with a thickness of ~50 nm was observed on the PTFE fiber surfaces **(Fig 2a** and **2b)**. The surface structure and porosity of the PTFE were maintained after the coating process. This structure is favourable for fast and extensive vapor diffusion and can facilitate good water evaporation performance (Lu et al., 2019). Energy-dispersive X-ray spectroscopy (EDS) analysis (**Fig. S5**) and elemental mapping (**Fig. 2c**) confirm the existence and the distribution of Au nanolayer homogeneously on the PTFE membrane surface. Additionally, XPS analysis was conducted to investigate the elemental composition and electronic structure of the Au-PTFE membrane surface. The XPS survey spectrum confirms the presence of Au, C, F and O (**Fig. 2d)**. High-resolution XPS analysis revealed narrow doublet peaks of Au $4f_{5/2}$ (84.12 eV) and Au $4f_{7/2}$ (87.75 eV), separated by 5 eV (**Fig. 2e)**. The peaks at 680 eV and 284.59 eV match the F 1s, and C1s, respectively (Kiriarachchi et al., 2018; Saravanakumar et al., 2020). The weak peaks of F 1s, and C 1s suggest the successful Au nanolayer uniform coating on the PTFE membrane surface.

The surface wettability plays a vital role in the anti-salt properties of PTMs for solar seawater desalination (Ibrahim et al., 2021a). The dynamic wetting of water droplets on the pristine PTFE and gold deposited PTFE membrane were measured using a contact angle measurement (tensiometer) apparatus. The pristine PTFE membrane surface showed a water contact angle

of 145 ±3°, indicating that it is almost superhydrophobic (**Fig. 2f)**. The thin layer of gold on the PTFE surface has drastically reduced its wettability, with a water contact angle of 100 ±4° (**Fig. 2g)**. Theis hydrophobic behavior supported the self-floating ability of the membrane on water. In addition, it can act as an anti-salt property by repealing the salt ion crystallization on the evaporator surface, which is beneficial for the long-term durability of solar desalination.

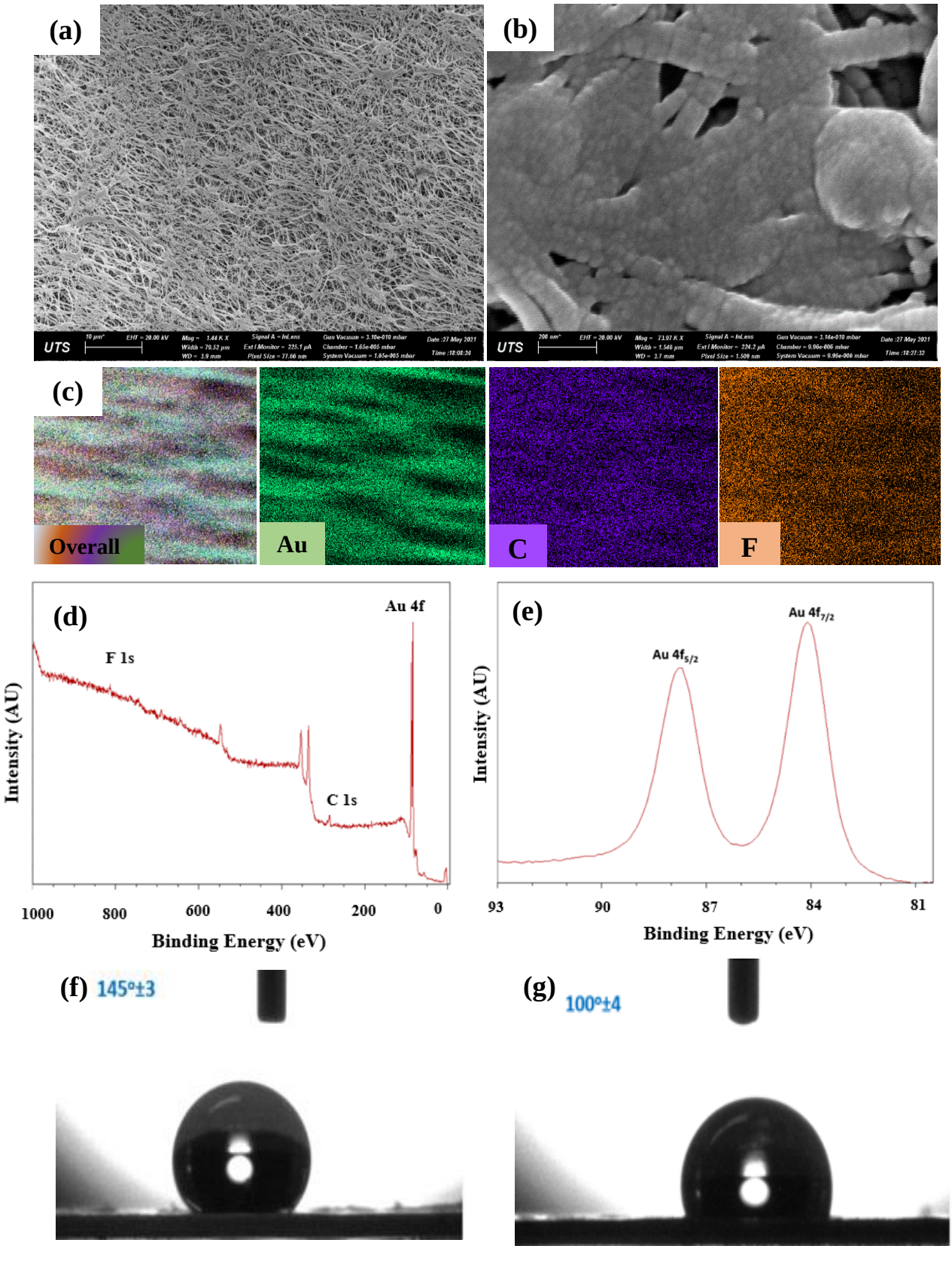


**Fig 2. (a)** Low and **(b)** high magnification SEM images of the Au/PTFE photothermal membrane; **(c)** EDS mapping results confirming the distribution of Au nanolayer on the PTFE

membrane surface; **(d)** X-ray photoelectron spectra (XPS) survey of Au-PTFE membrane; **(e)** High resolution XPS spectra confirming the existence of the Au 4f; and surface wettability test of the PTFE membrane (**f**) and Au nanolayer membrane (**g**) displaying hydrophobic properties, and reduction in hydrophobicity being observed after the gold nanolayer deposition.

### 3.2 Chemical and mechanical stability of Au nanolayer-PTFE membrane

PTMs with chemical stability and robust mechanical strength are essential for practical applications in SWE. The tensile strength and percentage strain results indicated that for pristine PTFE membrane, i.e., without the thin film gold coating, only 6.71 MPa and 33.9%, were obtained, respectively. After the coating process, the values have increased to 8.09 MPa, and 36.48%, respectively. This phenomenon can be explained by the strong adhesion of the coated Au nanolayer to the membrane, enhancing its mechanical properties. The gold did not detach or fall off from the surface of PTFE membrane. Furthermore, the chemical stability was assessed by heating the Au-PTFE membrane under acidic, basic, and oxidizing solution conditions at a temperature of 40 $^{o}$C for 30 hours, and then subjected the Au-PTFE membranes under sonication for 40 minutes. The EDS analysis revealed that the gold on the treated membranes maintained similar composition as with the original samples (**Fig. S6 a-d**) even after exposure to these harsh environments. This signifies that the magnetic sputtering method could be a superior technique to fabricate Au nanolayer-based solar absorber compared to those techniques reported in literature, such as electrospinning (Wu et al., 2019a) and dip-coating (Zhu et al., 2018). The obtained results demonstrated that the magnetic sputtering method resulted in nanolayer gold formation with remarkable adhesiveness on PTFE membrane. This could be a promising strategy for the fabrication of a stable photothermal membrane for solar-driven water purification.

### 3.3 Optical characteristics and solar-thermal conversion of gold nanolayer membrane

The structure-dependent light absorption characteristics of the pristine PTFE and the designed Au nanolayer-PTFE membranes were evaluated using a UV-Vis-NIR spectrometer in the wavelength range of 300-2500 nm (**Fig. 3a**). The inset image in **Fig. 4a** shows the reference solar spectrum (at AM 1.5 G) (Politano et al., 2017). The pristine PTFE displayed weak light absorption characteristics in the whole solar spectrum regions. In contrast, the coated PTFE membrane with Au nanolayer shows a much higher light absorption covering the whole solar spectrum region, with light absorption of ~ 80% in the UV region (300-400 nm), ~ 55-80% in the visible region (400-700 nm), and ~ 40-55% in the NIR region (700-2500 nm). Along with good light absorption characteristics of the prepared gold nanolayer PTFE membrane, surface plasmon resonance (SPR) effect from the gold nanolayer helps to generate heat in the PTMs for the effective water evaporation to occur. Plasmonic metals such as gold, due to the presence of high concentration of free carriers, enable free-carrier absorption (Zhao et al., 2020a). The plasmon-induced heat generation occurs when Au nanolayer is illuminated at their resonant wavelengths, which causes oscillation of the electron cloud of free electrons. The decay of the hot electrons through electron-electron scattering creates and redistributes the hot electron energy in the form of heat, which can rapidly increase the localized surface temperature of plasmonic Au (Kim et al.; Linic et al., 2015). Furthermore, the rough surface of the PTFE membrane and the holes with open and distributed channels play an effective role in reducing light reflection and can trap the photon capture (Lu et al., 2019). Hence, the absorption is considered as angle-independent due to the potential multiple scattering between the fibrous membrane (Zhu et al., 2018). This enhancement in the optical performance is beneficial for solar-thermal conversion for water evaporation application. The optical performance of our Au nanolayer-PTFE membrane is comparable with some reported optical characteristics of noble metal PTMs in SWE (Chen et al., 2018; Kiriarachchi et al., 2018; Huang et al., 2020b).

After the optical properties test, we designed a simple solar evaporator consisting of a Au nanolayer membrane (Au-PTFE) placed on top of a hydrophilic porous cellulose sponge (CS) (referred to as Au-PTFE@CS). The added CS has dual-function roles; (1) acting as thermal insulator where it can localize the heat at the air/water interface, and can reduce the downward heat losses, and, (2) it helps in supplying water to the top hydrophobic photothermal Au-PTFE. This simple combination design allowed fast and continuous water supply from the bulk water to the top hydrophobic Au nanolayer-PTFE membrane. Meanwhile, the hydrophobic Au-PTFE can repeal the salt formation resulting in excellent salt ions rejections with long-term durability and stable performance. For comparison, a pristine PTFE membrane was examined as well as a free-standing Au nanolayer membrane (without CS), and a DI water only condition.

The surface temperature change of the designed solar evaporator was monitored over time using an IR camera under 1 sun (1 kW $m^{-2}$) illumination. As illustrated in **Fig. 3b** and **3c**, the surface temperature of the pristine PTFE membrane only showed a slight increase in temperature from 22.1 $^{o}$C to 24.8 $^{o}$C within 10 min. In contrast, the surface temperature of the Au-PTFE@CS rapidly increased from an ambient temperature of 25.2 $^{o}$C to reach 30 $^{o}$C within 3 minutes of illumination and further rose to 33.2 ℃ after 10 min. In addition, without CS, the surface of free-standing Au nanolayer membrane increased to 29.3 $^{o}$C. The surface temperature of the Au-PTFE with CS is higher compared to without CS demonstrating its excellent solar light-to-heat conversion. One reason for this is due to CS support, which acts as thermal insulator and heat localizer at the air-water interface. To further investigate the effectiveness of the CS in localizing heat and reducing the heat transmittance to bulk water, we measured the bulk water temperature using a thermocouple. The side-view image using IR camera was also used to visualize the heat distribution on the side of the solar evaporator. The thermal images of Au-PTFE with CS revealed that heat is localized with low transmission to the bulk water (**Fig. 3d**). Furthermore, the bulk water temperature change was relatively low with an

increase in temperature from 25.6 °C to 26.5 °C (i.e., 0.9 °C difference). Meanwhile, without CS, the bulk water temperature increased from 25.6 °C to 30.7 °C, which indicated the fast conduction of heat to the water. These observations demonstrate the effectiveness of adding thermal insulation in localizing the heat at the air-water interface and minimizing the downward heat losses, which is beneficial for solar water evaporation application.

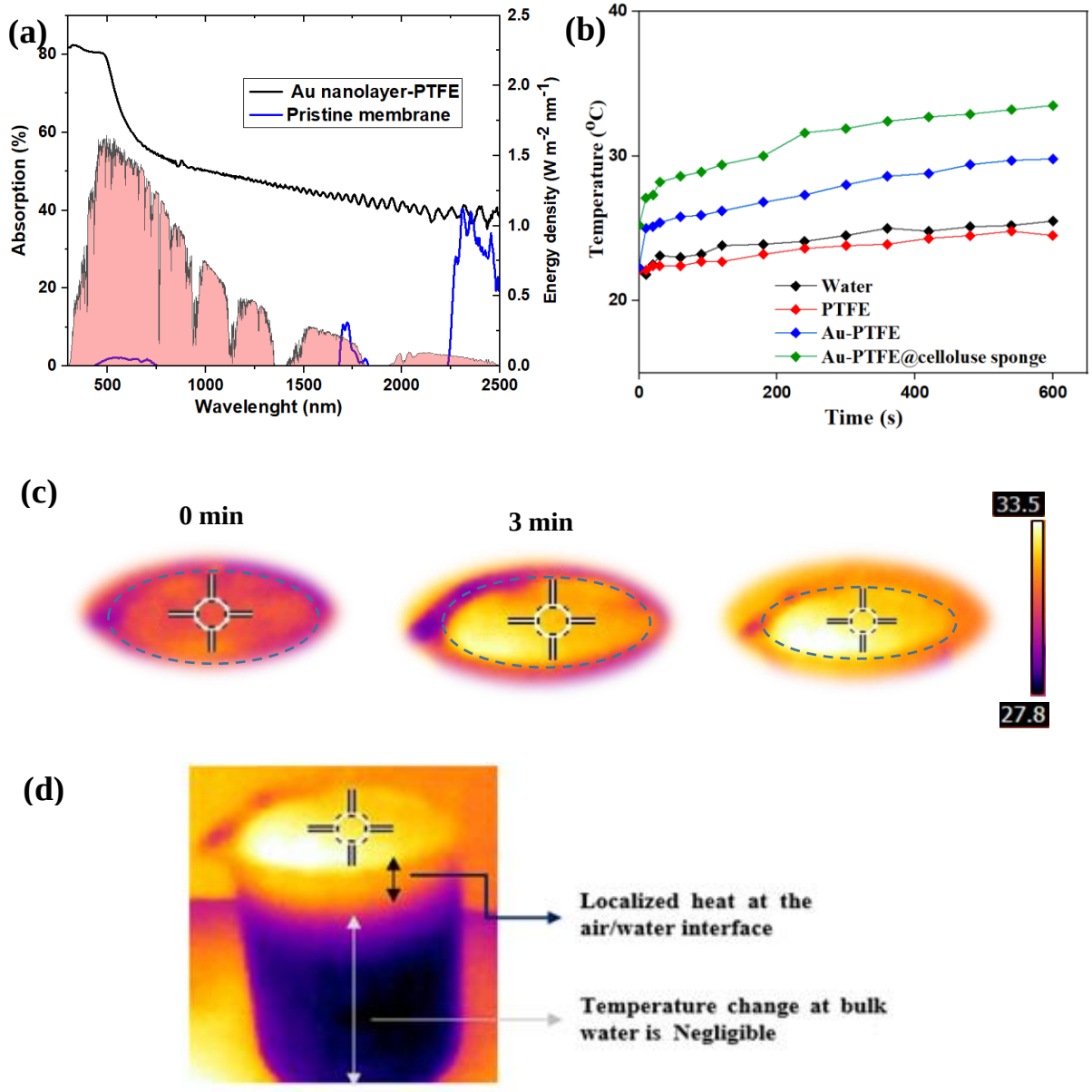


**Fig 3. Solar absorption and solar-thermal conversion. (a)** Light absorption characteristics of the Au nanolayer membrane in the UV-vis and NIR regions. **(b)** The temperature changes

of the Au-PTFE/CS, pristine PTFE membrane, and water only at 1-sun irradiation. **(c)** Infrared image of the heat distribution after surface exposure to 1 sun-irradiation from 0 to 10 minutes. **(d)** Infrared photo confirming the capability of the device to localize heat at the air-water interface.

### 3.4 Solar water evaporation performance

The solar water evaporation performance of the Au-PTFE/CS was investigated and compared to those of DIW, and a freestanding Au-membrane (without CS support), under 1 sun solar illumination. The solar heat-to-vapor efficiency ($\eta$) is calculated using the following equation (Shan et al., 2019; Zhao et al., 2020d):

$$\eta = \frac{\Delta m * He}{I * T} \times 100\%,$$

where $\Delta m$ refers to ($m_i - m_o$), $m_i$ is the water mass change ($kg/m^2$) under solar light, and $m_o$ is the water mass change ($kg/m^2$) at dark condition (without sunlight). *He* is the total vaporization enthalpy of the water-steam phase change ($kJ \cdot kg^{-1}$), *I* is the solar power energy density ($kW\ m^{-2}$), and T (h) is the irradiation period. The evaporation rates at the dark condition were 0.081, 0.072, and 0.078 kg $m^{-2}$ $h^{-1}$ for DIW, free-standing Au nanolayer-PTFE, and Au nanolayer-PTFE/CS, respectively (**Fig. S7**).

Under 1 sun illumination, the DIW displayed an evaporation rate of 0.314 kg $m^{-2}$ $h^{-1}$, corresponding to an evaporation efficiency of 14.8%. The evaporation rate was significantly increased after placing free-standing Au nanolayer membrane at the air/water interface to deliver evaporation rate of 0.64 kg $m^{-2}$ $h^{-1}$, corresponding to an efficiency of 35.6% which is ~2 times that of pure water. The vapor generation arises from the absorption of the solar light through the gold nanolayer which generates a sufficient heat at the air-water interface. It was noticed that the evaporation rate was further improved by placing cellulose sponge below the

Au nanolayer membrane to achieve an evaporation rate of 0.88 kg $m^{-2}$ $h^{-1}$, corresponding to an efficiency of ~ 49.5%. **Fig. 4a and 4b** display the water evaporation rate and solar- heat-to-vapor efficiency results in this work. The reason for such further increase is due to the presence of underlying hydrophilic CS, which offers great heat confinement and provides efficient solar heat utilization. In addition, it delivers sufficient and continuous water supply to the hydrophobic Au nanolayer membrane. The spaces between the hydrophobic Au nanolayer membranes facilitate vapor escaping. Meanwhile, without CS (free standing Au nanolayer), some of the generated heat by the Au nanolayer membrane were transmitted to the bulk water via heat conduction, resulting in lower water evaporation. **Fig. 4c** describes the designed device and the evaporation process. The obtained evaporation rate in this study is comparable to some reported studies in the literature (**Table S1**). The effect of the CS thickness on the water evaporation was investigated to find the optimal thickness. At 0.6 cm CS thickness, it generated a water evaporation rate of 0.82 kg $m^{-2}$ $h^{-1}$ at one sun intensity, while the 1.6 cm CS thickness resulted to an evaporation rate of 0.86 kg $m^{-2}$ $h^{-1}$, which is similar to the 1.2 cm thickness. Hence, we chose 1.2 cm cellulose sponge as the optimized thickness in our current study (see **Fig. S8**).

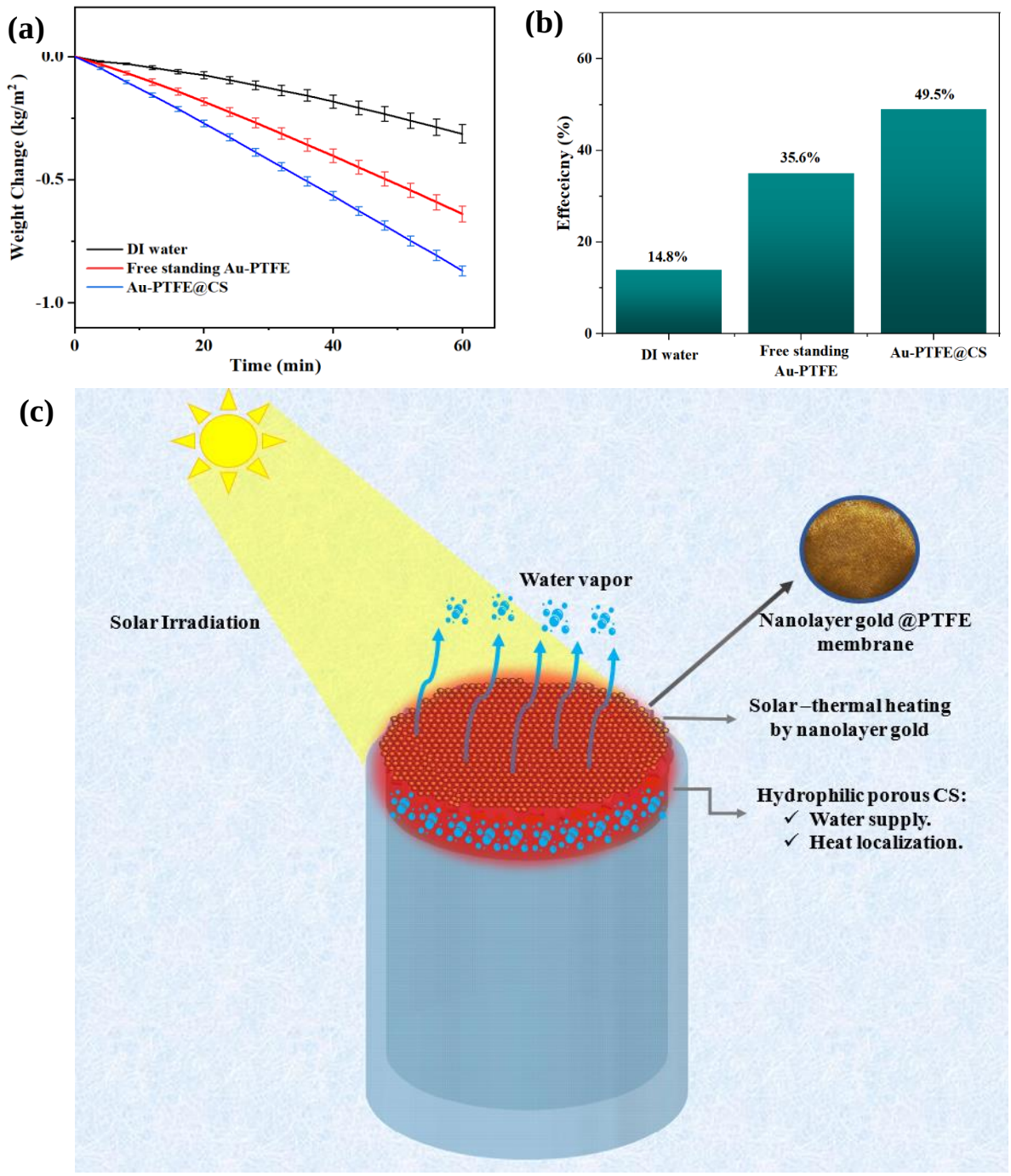


**Fig 4. (a)** Weight change of DIW, free standing Au-PTFE, and Au-PTFE supported CS under 1 sun intensity, **(b)** their corresponding solar conversion efficiency, and **(c)** schematic illustration of the solar conversion and vapour generation process of Au nanolayer membrane on CS based solar evaporator.

### 3.5 Solar desalination performance

The feasibility of the Au-PTFE membrane for solar water desalination was also investigated. For the desalination tests, real seawater samples from Cronulla Beach, Sydney were used. Interestingly, the Au nanolayer-PTFE membrane displayed a seawater evaporation rate of 0.859 kg $m^{-2}$ $h^{-1}$, close to the evaporation rate of DI water of 0.88 kg $m^{-2}$ $h^{-1}$ (**Fig. S10**). In order to investigate the capability of the evaporator system for generating potable water, the evaporated water was condensed, collected and analyzed using ICP-MS and compared to the original seawater. Schematic illustration of the device used for the water condensation and collection is provided in **Fig. 5a and Fig. S9**. The results indicated that a high amount of the salt ions $Na^+$, $K^+$, $Ca^{2+}$, and $Mg^{2+}$ in the purified water were significantly decreased to 7.79, 0.60, 0.62, and 0.86 mg/L, respectively compared to their respective initial concentrations of 8750, 1043.7, 348.3 and 398.3 mg/L (**Fig. 5b**). The obtained values are below the standard for drinking water required by World Health Organization (WHO) and the U.S. Environmental Protection Agency (EPA) (i.e., $Na^+$: 200 mg/L, $Ca^{2+}$: 75 mg/L, $K^+$: 12 mg/L, and $Mg^{2+}$: 50 mg/L) (WHO, 1993; EPA, 2012). This result proves the capability of Au nanolayer-PTFE membrane-based solar evaporator for producing drinking water.

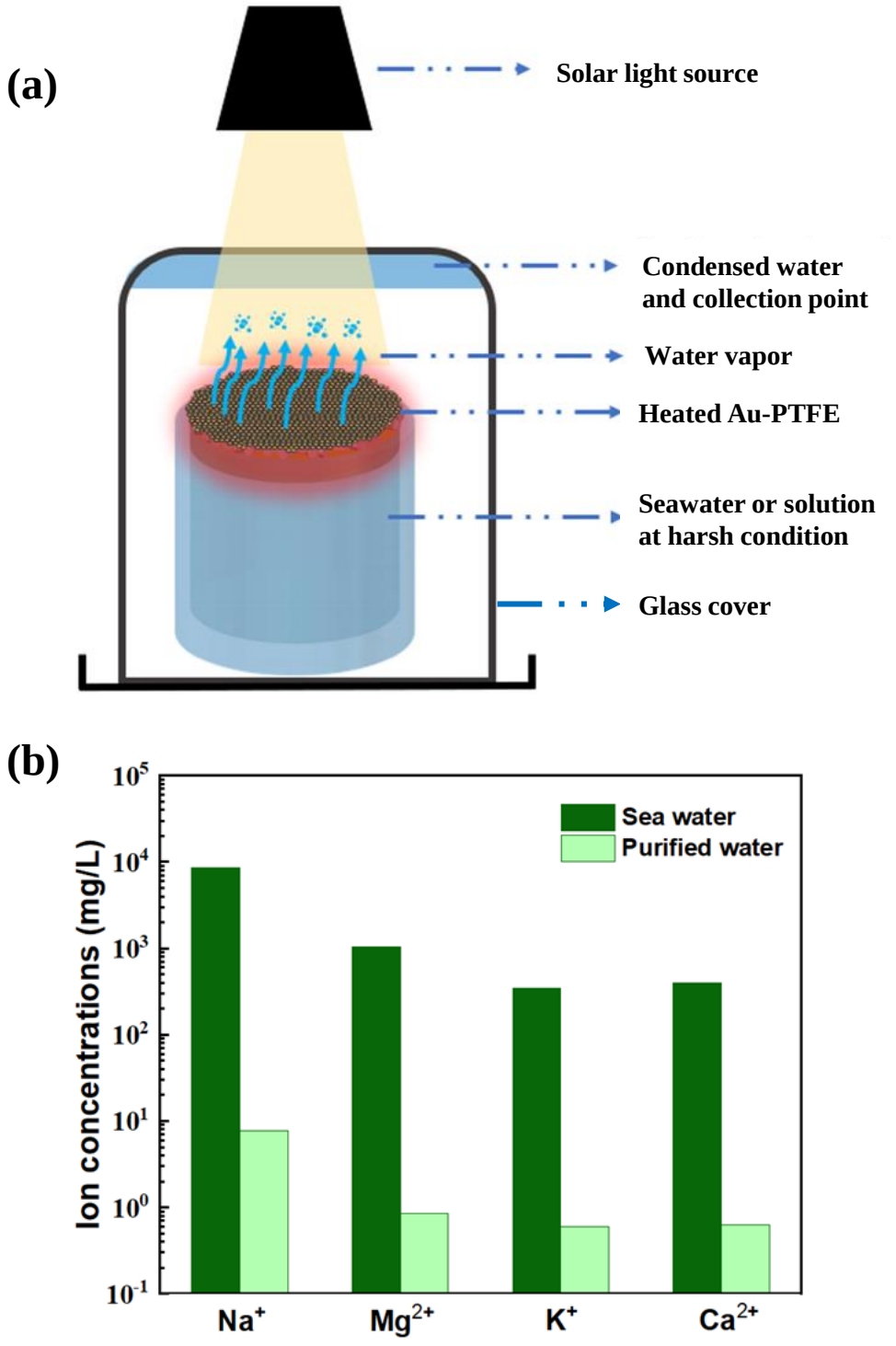


**Fig. 5 (a)** Schematic of the purpose-built device for collecting water vapour. **(b)** The concentrations of ions ($Na^+$, $K^+$, $Ca^{2+,}$ and $Mg^{2+}$) in seawater collected from Cronulla Beach showing a high reduction in ion concentrations before and after the desalination process.

### 3.6 Durability and stability test

The durability and stability of the solar evaporator system are essential factors for practical solar water evaporation applications. The salt formation on the solar absorbers will cause a significant decrease in the light absorption of the photothermal materials, causing a lower evaporation surface (Ibrahim et al., 2020; Ibrahim et al., 2021a). Therefore, it should be addressed before implementing this technology for practical application. The self-cleaning capability of the Au-PTFE@CS evaporator was investigated by placing 2.5 g of salt on the top of the membrane (see **Fig. 6**). After sunlight irradiation at 1 sun intensity, the salt gradually disappeared with continuous vapor flow through the holes between the coated fibre of Au-PTFE membrane until no salt was observed after 2.5 hours (**Fig. 6**). The self-cleaning ability of the designed evaporators can be ascribed to the spaces between the heated fibres in Au-PTFE membranes which allows continuous vapor flow for chemical advection and diffusion induced by salt concentration gradient, resulting in salt dissolution (Irshad et al., 2021; Zhou et al., 2021). In addition, the hydrophilic open pores CS allows formation of thin layer water underneath of the Au nanolayer membrane resulting in sufficient water supply and leading to dissolution of the solid NaCl.

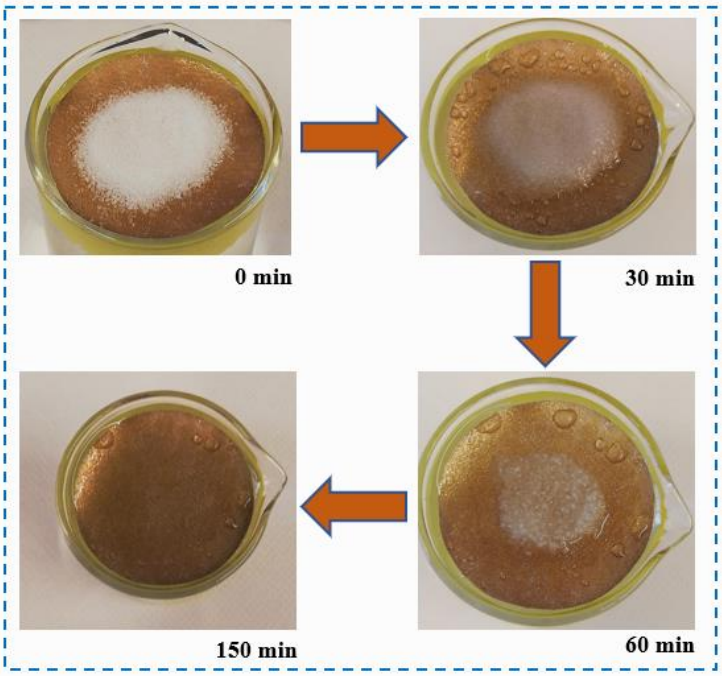

**Fig 6.** Photo-image of salt-dissolution of nanolayer Au-PTFE based solar evaporator after adding 2.5 g NaCl, demonstrating a self-cleaning property

To examine the durability of Au nanolayer-PTFE membrane for solar desalination, we conducted the evaporation test using natural seawater and high salinity brine (150 g/L NaCl) as model brine solution. The test was carried out for 10 continuous cycles (1 h/cycle) under one sun intensity. Interestingly, excellent reusability with stable performance over 10 cycles was demonstrated, with only a slight decrease in the evaporation rate of 0.85 kg $m^{-2}$ $h^{-1}$ for seawater, to 0.82 kg $m^{-2}$ $h^{-1}$ for the brine solution (150 g/L NaCl) (**Fig. 7a and Fig. S10**). The slight reduction in the evaporation rate for brine solution is attributed to the decrease in vapor pressure of the brine solution (Zhang et al., 2015; Xu et al., 2019; Luo et al., 2021). The above-mentioned results indicate excellent salt resistance due to the continuous water supply through CS, which also provides a thin layer of water. In addition to that, due to the surface hydrophobicity of the Au nanolayer-PTFE membrane, no noticeable salt was formed. This result implies that MS technique is a reliable technology to fabricate a stable nanolayer photothermal membrane for seawater desalination, especially towards high-salinity solution with anti-fouling properties. We further extend the durability study to harsh chemical conditions, under acidic (0.1M $H_2SO_4$, pH = 1), basic (0.1M KOH, pH = 13), and oxidizing conditions (0.1M $HNO_3$), corresponding to ionic strengths (*I*) of 0.3 M, 0.1 M, and 0.1 M, respectively. The ion concentrations of $SO_4^{2-}$, $K^+$ and $NO_3^-$ were reduced to 0.4649, 6.41121, and 0.5434, mg $L^{-1}$, respectively, revealing remarkable efficiency in obtaining clean water even under harsh conditions (**Fig. 7b**). Besides, the evaporation rate indicates that the fabricated Au nanolayer membrane possess an excellent evaporation rate of 0.80 kg $m^{-2}$ $h^{-1}$ (under 0.1 M $H_2SO_4$), 0.85 kg $m^{-2}$ $h^{-1}$ (under 0.1 M KOH), and 0.85 kg $m^{-2}$ $h^{-1}$ (under 0.1 M $HNO_3$), which are close to that of the corresponding DI water evaporation rate (0.88 kg $m^{-2}h^{-1}$), suggesting

its stable evaporation performances **(Fig. S11)**. The slight reduction in evaporation rate of $H_2SO_4$ is attributed to the higher *I* value compared to $HNO_3$ and KOH. Additionally, the cycling stability was carried out for 5 cycles (1 h test per 1 cycle). Ultimately, the results showed excellent reusability with stable performance (**Fig. 7c**). This good performance are attributed to three main reasons: (i) the chemical resistivity of the gold (Hammer and Norskov, 1995; Badawy et al., 2010; Kiriarachchi et al., 2018), (ii) the superior mechanical strength of the Au nanolayer-PTFE membrane, and (iii) the strong adhesiveness and attachment of the thin layer Au on the PTFE membrane. Therefore, it can be concluded that the fabricated gold membrane allowed efficient steam diffusion, minimized salt accumulation, and maintained membrane cycle stability under harsh environments.

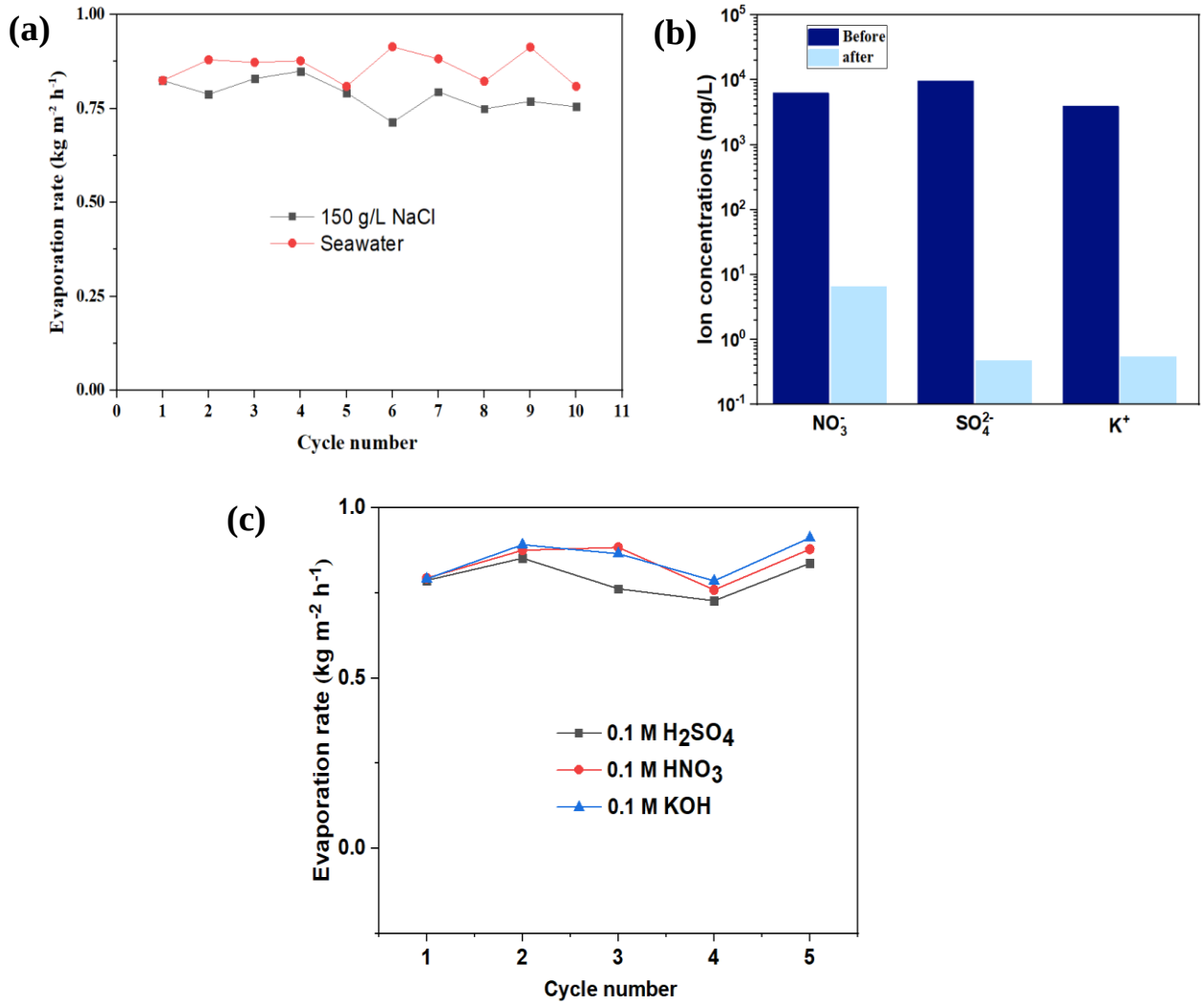

**Figure 7. (a)** Cycling performance of the Au nanolayer membrane using seawater, revealing stable evaporation rate for a period of 10 cycles. **(b)** Ion concentrations ($SO_4^{2-}$, $NO_3^-$, and $K^+$) before and after the evaporation showing the capability of Au nanolayer membrane for excellent ions rejection under harsh environment. **(c)** The cycling stability under acidic, basic and oxidizing conditions for a period of 5 cycles.

## Conclusion

This study demonstrates the feasibility of applying a magnetron sputtering method to fabricate a novel Au nanolayer membrane with robust mechanical strength and chemical stability for SWE applications. Detailed morphological, structural and material analysis techniques indicated that gold nanolayer were formed and homogeneously coated on the fiber of PTFE membrane surface. The resultant Au nanolayer membranes achieved a water evaporation rate of 0.88 kg $m^{-2}$ $h^{-1}$, which corresponds to an efficiency of 49.5%, under 1-sun irradiation. Also, this system revealed a high rejection rate of salt ions from seawater with a removal efficiency of 99.9%, meeting the standard required for drinking water. Furthermore, the adhesiveness and the strong attachment of the thin film Au nanolayer on the membrane resulted in excellent durability and stability even under harsh conditions. Our proposed novel strategy may open up a new pathway for designing a highly stable nanolayer thin-film PTM for solar water purification.

## Acknowledgments

Idris Ibrahim is grateful for the financial support from the Australian Government through the International Research Training Program (IRTP) Scholarship for his PhD studies. Dong Han Seo acknowledges the support of UTS Chancellor's Postdoctoral Research Fellowship scheme. Hokyong Shon expresses gratitude for the support by the Korea Environment Industry &

Technology Institute (KEITI) through Industrial Facilities & Infrastructure Research Program, funded by Korea Ministry of Environment (MOE) (1485016424), and also from the Australian Research Council (ARC) support. Leonard Tijing and team appreciate the support from the UTS Cross-Faculty Collaboration Scheme (PRO21-12429). Authors would also like to acknowledge Dr. Alaina Ammit and Dr. Katie McBean for their assistance in providing the laboratory access.

## CrediT authorship contribution statement

**Idris Ibrahim:** Conceptualization, methodology, writing-original draft, review & editing Visualization, data curation, Investigation. **Dong Han Seo:** Conceptualization, supervision, visualization, data curation, review & editing. **Alexander Angeloski**: Methodology, review & editing. **MJ Park:** Methodology. **Andrew McDonagh:** Supervision, data curation, review & editing. **Avi Bendavid:** Conceptualization, methodology, investigation. **Hokyong Shon:** Supervision, resources, review & editing. **Leonard Tijing:** Supervision, resources, investigation, planning, data curation, visualization, review & editing.

## References

Badawy, A.M.E., Luxton, T.P., Silva, R.G., Scheckel, K.G., Suidan, M.T., Tolaymat, T.M., 2010. Impact of environmental conditions (pH, ionic strength, and electrolyte type) on the surface charge and aggregation of silver nanoparticles suspensions. Environ. Sci. Technol. 44, 1260-1266. https://doi.org/10.1021/es902240k.

Barbosa, A.I., Borges, J., Meira, D.I., Costa, D., Rodrigues, M.S., Rebelo, R., Correlo, V.M., Vaz, F., Reis, R.L., 2019. Development of label-free plasmonic Au-$TiO_2$ thin film immunosensor devices. Mater. Sci. Eng. C. 100, 424-432. https://doi.org/10.1016/j.msec.2019.03.029.

Chang, Y., Wang, Z., Shi, Y.-e., Ma, X., Ma, L., Zhang, Y., Zhan, J., 2018. Hydrophobic $W_{18}O_{49}$ mesocrystal on hydrophilic PTFE membrane as an efficient solar steam generation device under one sun. J. Mater. Chem. A. 6, 10939-10946. https://doi.org/10.1039/C8TA02700E.

Chen, J., Yin, J.L., Li, B., Ye, Z., Liu, D., Ding, D., Qian, F., Myung, N.V., Zhang, Q., Yin, Y., 2020. Janus evaporators with self-recovering hydrophobicity for salt-rejecting interfacial solar desalination. ACS Nano 14, 17419-17427. https://doi.org/10.1021/acsnano.0c07677.

Chen, L., Xu, P., Kota, K., Kuravi, S., Wang, H., 2021a. Solar distillation of highly saline produced water using low-cost and high-performance carbon black and airlaid paper-based evaporator (CAPER). Chemosphere 269, 129372. https://doi.org/10.1016/j.chemosphere.2020.129372.

Chen, M., Wu, Y., Song, W., Mo, Y., Lin, X., He, Q., Guo, B., 2018. Plasmonic nanoparticle-embedded poly (p-phenylene benzobisoxazole) nanofibrous composite films for solar steam generation. Nanoscale 10, 6186-6193. https://doi.org/10.1039/C8NR01017J.

Chen, Z., Luo, Y., Li, Q., Chen, X., 2021b. Microgroove-structured PDA/PEI/PPy@PI-MS photothermal aerogel with a multilevel water transport network for highly salt-rejecting solar-driven interfacial evaporation. ACS Appl. Mater. Interfaces. 13, 40531-40542. https://doi.org/10.1021/acsami.1c09155.

U.S. Environmental Protection Agency (EPA), 2012. 2012 Edition of the drinking water standards and health advisories. EPA 822-S-12-001.

Ghafurian, M.M., Niazmand, H., Ebrahimnia-Bajestan, E., Taylor, R.A., 2020a. Wood surface treatment techniques for enhanced solar steam generation. Renew. Energy. 146, 2308-2315. https://doi.org/10.1016/j.renene.2019.08.036.

Ghafurian, M.M., Niazmand, H., Goharshadi, E.K., Zahmatkesh, B.B., Moallemi, A.E., Mehrkhah, R., Mahian, O., 2020b. Enhanced solar desalination by delignified wood coated with bimetallic Fe/Pd nanoparticles. Desalination 493, 114657. https://doi.org/10.1016/j.desal.2020.114657.

Grammatikopoulos, S., Pappas, S., Dracopoulos, V., Poulopoulos, P., Fumagalli, P., Velgakis, M., Politis, C., 2013. Self-assembled Au nanoparticles on heated Corning glass by DC magnetron sputtering: size-dependent surface plasmon resonance tuning. J Nanopart Res. 15, 1-8. https://doi.org/10.1007/s11051-013-1446-3.

569 Greene, J.E., 2017. Tracing the recorded history of thin-film sputter deposition: From the 1800s to 2017.
570 J. Vac. Sci. Technol A 35, 05C204. https://doi.org/10.1116/1.4998940.
571 Hammer, B., Norskov, J.K., 1995. Why gold is the noblest of all the metals. Nature 376, 238-240.
572 https://doi.org/10.1038/376238a0.
573 He, J., Zhang, Z., Xiao, C., Liu, F., Sun, H., Zhu, Z., Liang, W., Li, A., 2020. High-performance salt-
574 rejecting and cost-effective superhydrophilic porous monolithic polymer foam for solar steam
575 generation. ACS Appl. Mater. Interfaces. 12, 16308-16318.
576 https://doi.org/10.1021/acsami.9b22832.
577 Huang, L., Ling, L., Su, J., Song, Y., Wang, Z., Tang, B.Z., Westerhoff, P., Ye, R., 2020a. Laser-
578 engineered graphene on wood enables efficient antibacterial, anti-salt-fouling, and lipophilic-
579 matter-rejection solar evaporation. ACS Appl. Mater. Interfaces. 12, 51864-51872.
580 https://doi.org/10.1021/acsami.0c16596.
581 Huang, Z., Li, S., Cui, X., Wan, Y., Xiao, Y., Tian, S., Wang, H., Li, X., Zhao, Q., Lee, C.-S., 2020b.
582 A broadband aggregation-independent plasmonic absorber for highly efficient solar steam
583 generation. J. Mater. Chem. A. 8, 10742-10746. https://doi.org/10.1039/D0TA01980A.
584 Ibrahim, I., Bhoopal, V., Seo, D.H., Afsari, M., Shon, H.K., Tijing, L.D., 2021a. Biomass-based
585 photothermal materials for interfacial solar steam generation: A review. Mater. Today Energy. 21,
586 100716. https://doi.org/10.1016/j.mtener.2021.100716.
587 Ibrahim, I., Seo, D.H., Angeloski, A., McDonagh, A., Shon, H.K., Tijing, L.D., 2021b. 3D microflowers
588 CuS/$Sn_2S_3$ heterostructure for highly efficient solar steam generation and water purification. Sol.
589 Energy Mater. Sol. Cells 232, 111377. https://doi.org/10.1016/j.solmat.2021.111377.
590 Ibrahim, I., Seo, D.H., McDonagh, A.M., Shon, H.K., Tijing, L., 2020. Semiconductor photothermal
591 materials enabling efficient solar steam generation toward desalination and wastewater treatment.
592 Desalination 500, 114853. https://doi.org/10.1016/j.desal.2020.114853.
593 Irshad, M.S., Wang, X., Abbas, A., Yu, F., Li, J., Wang, J., Mei, T., Qian, J., Wu, S., Javed, M.Q., 2021.
594 Salt-resistant carbon dots modified solar steam system enhanced by chemical advection. Carbon
595 176, 313-326. https://doi.org/10.1016/j.carbon.2021.01.140.

596 Kim, M., Lee, J.-H., Nam, J.-M., 2019. Plasmonic photothermal nanoparticles for biomedical
597 applications. Adv. Sci. 6, 1900471. https://doi.org/10.1002/advs.201900471.
598 Kiriarachchi, H.D., Awad, F.S., Hassan, A.A., Bobb, J.A., Lin, A., El-Shall, M.S., 2018. Plasmonic
599 chemically modified cotton nanocomposite fibers for efficient solar water desalination and
600 wastewater treatment. Nanoscale 10, 18531-18539. https://doi.org/10.1039/C8NR05916K.
601 Li, D., Zhang, X., Zhang, S., Wang, D., Wang, Z., Liu, Y., Yu, X., Zhao, Q., Xing, B., 2021. A flexible
602 and salt-rejecting electrospun film-based solar evaporator for economic, stable and efficient solar
603 desalination and wastewater treatment. Chemosphere 267, 128916.
604 https://doi.org/10.1016/j.chemosphere.2020.128916.
605 Li, J., Du, M., Lv, G., Zhou, L., Li, X., Bertoluzzi, L., Liu, C., Zhu, S., Zhu, J., 2018a. Interfacial solar
606 steam generation enables fast-responsive, energy-efficient, and low-cost off-grid sterilization.
607 Adv. Mater. 30, 1805159. https://doi.org/10.1002/adma.201805159.
608 Li, J., Wang, X., Lin, Z., Xu, N., Li, X., Liang, J., Zhao, W., Lin, R., Zhu, B., Liu, G., 2020. Over 10
609 kg $m^{-2}$ $h^{-1}$ evaporation rate enabled by a 3D interconnected porous carbon foam. Joule 4, 928-937.
610 https://doi.org/10.1016/j.joule.2020.02.014.
611 Li, X., Min, X., Li, J., Xu, N., Zhu, P., Zhu, B., Zhu, S., Zhu, J., 2018b. Storage and recycling of
612 interfacial solar steam enthalpy. Joule 2, 2477-2484. https://doi.org/10.1016/j.joule.2018.08.008.
613 Linic, S., Aslam, U., Boerigter, C., Morabito, M., 2015. Photochemical transformations on plasmonic
614 metal nanoparticles. Nat. Mater. 14, 567. https://doi.org/10.1038/nmat4281.
615 Liu, F., Liang, W., Wang, C., He, J., Xiao, C., Zhu, Z., Sun, H., Li, A., 2021. Superwetting monolithic
616 hypercrosslinked polymers nanotubes with high salt-resistance for efficient solar steam generation.
617 Sol. Energy Mater. Sol. Cells 221, 110913. https://doi.org/10.1016/j.solmat.2020.110913.
618 Lu, Q., Yang, Y., Feng, J., Wang, X., 2019. Oxygen-defected molybdenum oxides hierarchical
619 nanostructure constructed by atomic-level thickness nanosheets as an efficient absorber for solar
620 steam generation. Solar RRL 3, 1800277. https://doi.org/10.1002/solr.201800277.
621 Luo, Y.-Q., Song, F., Wu, J.-M., Wang, F., Wang, X.-L., Wang, Y.-Z., 2021. A nature-inspired
622 suspended solar evaporator for water desalination of high-salinity brines. Chem. Eng. J. 421,
623 129824. https://doi.org/10.1016/j.cej.2021.129824.

624 Neumann, O., Urban, A.S., Day, J., Lal, S., Nordlander, P., Halas, N.J., 2013. Solar vapor generation
625 enabled by nanoparticles. ACS Nano 7, 42-49. https://doi.org/10.1021/nn304948h.
626 World Health Organization (WHO), 1993. Guidelines for drinking-water quality (1993). Workld Health
627 Organiation.
628 Peng, F., Xu, J., Bai, X., Feng, G., Zeng, X., Raihan, M.R.I., Bao, H., 2021. A janus solar evaporator
629 with 2D water path for highly efficient salt-resisting solar steam generation. Sol. Energy Mater.
630 Sol. Cells 221, 110910. https://doi.org/10.1016/j.solmat.2020.110910.
631 Pinho, A.C., Piedade, A.P., 2013. Zeta potential, contact angles, and AFM imaging of protein
632 conformation adsorbed on hybrid nanocomposite surfaces. ACS Appl. Mater. Interfaces. 5, 8187-
633 8194. https://doi.org/10.1021/am402302r.
634 Politano, A., Argurio, P., Di Profio, G., Sanna, V., Cupolillo, A., Chakraborty, S., Arafat, H.A., Curcio,
635 E.J.A.M., 2017. Photothermal membrane distillation for seawater desalination. Adv. Mater. 29,
636 1603504. https://doi.org/10.1002/adma.201603504.
637 Saravanakumar, K., Mariadoss, A.V.A., Sathiyaseelan, A., Wang, M.-H., 2020. Synthesis and
638 characterization of nano-chitosan capped gold nanoparticles with multifunctional bioactive
639 properties. Int. J. Biol. Macromol. 165, 747-757. https://doi.org/10.1016/j.ijbiomac.2020.09.177.
640 Shan, X., Lin, Y., Zhao, A., Di, Y., Hu, Y., Guo, Y., Gan, Z., 2019. Porous reduced graphene
641 oxide/nickel foam for highly efficient solar steam generation. Nanotechnology 30, 425403.
642 https://doi.org/10.1088/1361-6528/ab3127.
643 Shi, L., Wang, X., Hu, Y., He, Y., Yan, Y., 2020. Solar-thermal conversion and steam generation: a
644 review. Appl. Therm. Eng. 179, 115691.
645 Tao, P., Ni, G., Song, C., Shang, W., Wu, J., Zhu, J., Chen, G., Deng, T., 2018. Solar-driven interfacial
646 evaporation. Nat. energy. 3, 1031-1041. https://doi.org/10.1038/s41560-018-0260-7.
647 Wang, F., Hu, Z., Fan, Y., Bai, W., Wu, S., Sun, H., Zhu, Z., Liang, W., Li, A., 2020. Salt-rejection
648 solar absorbers based on porous ionic polymers nanowires for desalination. Macromol. Rapid
649 Commun. 42, 2000536. https://doi.org/10.1002/marc.202000536.
650 Wang, S., Fan, Y., Wang, F., Su, Y., Zhou, X., Zhu, Z., Sun, H., Liang, W., Li, A., 2021. Potentially
651 scalable fabrication of salt-rejection evaporator based on electrogenerated polypyrrole-coated

nickel foam for efficient solar steam generation. Desalination 505, 114982. https://doi.org/10.1016/j.desal.2021.114982.

Wei, N., Li, Z., Li, Q., Yang, E., Xu, R., Song, X., Sun, J., Dou, C., Tian, J., Cui, H., 2021. Scalable and low-cost fabrication of hydrophobic PVDF/$WS_2$ porous membrane for highly efficient solar steam generation. J. Colloid Interface Sci. 588, 369-377. https://doi.org/10.1016/j.jcis.2020.12.084.

Wu, T., Li, H., Xie, M., Shen, S., Wang, W., Zhao, M., Mo, X., Xia, Y., 2019a. Incorporation of gold nanocages into electrospun nanofibers for efficient water evaporation through photothermal heating. Mater. Today Energy. 12, 129-135. https://doi.org/10.1016/j.mtener.2018.12.008.

Wu, X., Chen, G.Y., Owens, G., Chu, D., Xu, H., 2019b. Photothermal materials: a key platform enabling highly efficient water evaporation driven by solar energy. Mater. Today Energy. 12, 277-296. https://doi.org/10.1016/j.mtener.2019.02.001.

Xu, N., Li, J., Wang, Y., Fang, C., Li, X., Wang, Y., Zhou, L., Zhu, B., Wu, Z., Zhu, S., 2019. A water lily–inspired hierarchical design for stable and efficient solar evaporation of high-salinity brine. Sci. Adv. 5, eaaw7013. https://doi.org/10.1126/sciadv.aaw7013.

Xu, W., Hu, X., Zhuang, S., Wang, Y., Li, X., Zhou, L., Zhu, S., Zhu, J., 2018. Flexible and salt resistant Janus absorbers by electrospinning for stable and efficient solar desalination. Adv. Energy Mater. 8, 1702884. https://doi.org/10.1002/aenm.201702884.

Zhang, C., Liang, H.Q., Xu, Z.K., Wang, Z., 2019. Harnessing solar-driven photothermal effect toward the water–energy nexus. Adv Sci 6, 1900883. https://doi.org/10.1002/advs.201900883.

Zhang, J., Borg, M.K., Sefiane, K., Reese, J.M., 2015. Wetting and evaporation of salt-water nanodroplets: A molecular dynamics investigation. P Phys. Rev. E. 92, 052403. https://doi.org/10.1103/PhysRevE.92.052403.

Zhao, F., Guo, Y., Zhou, X., Shi, W., Yu, G., 2020a. Materials for solar-powered water evaporation. Nat Rev Mater 5, 388-401. https://doi.org/10.1038/s41578-020-0182-4.

678 Zhao, H.-Y., Zhou, J., Yu, Z.-L., Chen, L.-F., Zhan, H.-J., Zhu, H.-W., Huang, J., Shi, L.-A., Yu, S.-
679 H., 2020b. Lotus-inspired evaporator with Janus wettability and bimodal pores for solar steam
680 generation. Cell Reports Physical Sci 1, 100074. https://doi.org/10.1016/j.xcrp.2020.100074.
681 Zhao, Q., Huang, Z., Tian, S., Cui, X., Wan, Y., Li, X., Xiao, Y., Li, S., Lee, C.-S., 2020c. Superwetting
682 $B_4C$ bilayer foam for high cost-performance solar water purification. Mater Today Energy 18,
683 100498. https://doi.org/10.1016/j.mtener.2020.100498.
684 Zhao, S., Chen, L., Zhang, C., Hasi, Q.-M., Zhang, L., Luo, X., Li, A., 2020d. Functional oil-repellent
685 photothermal materials based on nickel foam for efficient solar steam generation. Sol. Energy
686 Mater. Sol. Cells 214, 110574. https://doi.org/10.1016/j.solmat.2020.110574.
687 Zhou, H., Xue, C., Chang, Q., Yang, J., Hu, S., 2021. Assembling carbon dots on vertically aligned
688 acetate fibers as ideal salt-rejecting evaporators for solar water purification. Chem. Eng. J. 421,
689 129822. https://doi.org/10.1016/j.cej.2021.129822.
690 Zhu, M., Li, Y., Chen, F., Zhu, X., Dai, J., Li, Y., Yang, Z., Yan, X., Song, J., Wang, Y., 2018.
691 Plasmonic wood for high-efficiency solar steam generation. Adv. Energy Mater. 8, 1701028.
692 https://doi.org/10.1002/aenm.201701028.

693